Journal of Applied Fluid Mechanics, Vol. 12, No. 3, pp. 831-843, 2019.
Available online at www.jafmonline.net, ISSN 1735-3645, EISSN 1735-3645.
DOI: 10.29252/jafm.12.03.29506

Numerical Study on the Effect of Temperature on Droplet Formation inside the Microfluidic Chip

F. Jiang[1†], Y. Xu[1], J. Song[2] and H. Lu[1]

[1] *School of Mechanical and Electrical Engineering, Guangzhou University, China*
[2] *Joining Technology Group, Singapore Institute of Manufacturing Technology, Singapore*

†*Corresponding Author Email: jiangfan2008@gzhu.edu.cn*

(Received August 6, 2018; accepted October 16, 2018)

ABSTRACT

The flow-focusing method is a technology for microfluidic droplet control, and the temperature can effect on the droplet formation. In this study, the droplet formation in the flow-focusing method during the squeezing of dispersed phase by the continuous phase is simulated using CLSVOF, with the consideration of the effects of temperature on droplet size, shape and frequency. The simulation results are consistent with experimental data. The simulated results demonstrate that the droplet size increases with the increase of inlet phase temperature, while the shape regularity and forming frequency decrease, the maximum increase of droplet size is 16%, the biggest drop of droplets number is 29%, and the biggest drop of the roughness parameter is 5%. When the inlet temperatures of the continuous phase are not equal, dripping and jetting are observed in the flow regime of droplet dispersed phase. The mechanism of the temperature influence on droplet formation and the detailed process of droplet formation under different flow regimes are discussed. At the same time, the radial size of droplet breakup point under different flow regimes is compared. The simulation results provide insights in better selection of the control parameters for droplet formation technology.

Keywords: Numerical simulation; Droplet formation; Flow focusing; Temperature; CLSVOF.

NOMENCLATURE

a	dispersion phase inlet radiu
b	continuous phase inlet radius
Ca	capillary number
E	energy
F	the external body
g	gravitational constant
h	continuous phase inlet groove depth
I	the unit tensor
k_C	thermal conductivity
L	distance between the two arms of bend
n	a power-law index
p	pressure in the flow field
R	fillet radius of the bend
t	time
T	temperature
v	velocity
w	droplet shearing aperture
z	vertical distance
ρ	density
μ	viscosity
μ_q	viscosity of the qth phase
α	phase volume fraction
α_q	phase volume fraction of the q-th phase
γ_o	surface tension coefficient
$\bar{\bar{\tau}}_t$	the stress tensor for q-th phase
$\dot{\gamma}$	the shear rate
ΔT	temperature difference

1. INTRODUCTION

With the extensive adoption of Lab-on-a-Chip in areas like medical diagnostics (Zec *et al.*, 2014; Price and Paegel, 2015; Hung, 2016), screening of biological assays (Theberge, 2010; Vyawahare, 2010), single cell analysis (Schneider, 2013; Mashaghi, 2016; Evanko, 2008), food and feed industries (Neethirajan *et al.*, 2011), preparation of nanoparticles (Jahn *et al.*, 2008; Song *et al.*, 2010) and other special materials (Abou-Hassan *et al.*, 2010), microfluidic technology, which is a key supporting technology in Lab-on-a-Chip, has been of great interests to researchers (Li et al. 2008;

Basova and Foret, 2015; Bruijns *et al.*, 2016). The main components of the droplet formation device in microchannel include T-junction (Christopher and Anna, 2007; Bedram and Moosavi, 2013), flow focusing structure (Teo *et al.*, 2018; Wang *et al.*, 2017), and drop-on-demand (DOD) generator (Eslamian and Ashgriz, 2011). Because of the high frequency of monodisperse droplets produced by the flow focusing structure, many researches on droplet forming have been carried out based on this structure. For example, Fabian *et al.* (2016) applied a magnetic field around the liquid drop forming device, the experimental results showed that stronger magnetic field results in larger neck diameter of the droplet in the final stage of droplet formation, and the effects of physical properties of both continuous and dispersed phases and inflow velocity on the droplet size and forming frequency were investigated (Zie *et al.*, 2008; Anna *et al.*, 2006; Wang *et al.*, 2017; Zhu and Wang, 2017). Derzsi *et al.* (2013) found that increasing velocity ratio between continuous and dispersed phases reduces the droplet size. Meanwhile, four kinds of flow regimes were discovered in their experiment, i.e., without satellite, single satellite, multiple satellite, and jetting. They also found that as the viscosity of dispersed phase and the velocity ratio increase, the droplet flow regime transitions from dripping to jetting. In the study of droplet flow regime, Xu *et al.* (2008) detected that the capillary number of continuous phases is between 0.002 and 0.01 in their test when the droplet flow regime transitions from dripping to jetting. Chwalek *et al.* (2002) altered the surface tension and viscosity of the liquid through the changing temperature and used this method to control the deflection angle of liquid micro-jet. Nauyen *et al.* (2007) heated the fracture point of the formed droplet, and their experimental results indicated that the size of the formed droplet increases with the increase of the heating temperature. Further study by Tan *et al.* (2008) showed that as the temperature increases, there may exist three kinds of flow regimes, i.e. dripping, squeezing A and squeezing B, at the fracture point of the droplet.

With the advance in the computer simulation, many researchers have adopted numerical methods to investigate the mechanism behind the droplet formation. Qiu *et al.* (2010) numerically analyzed the droplet formation in the non-Newtonian fluid in a cross-flow microchannel, and is revealed that the rheological parameters of non-Newtonian fluid have a significant influence on the formation mechanism and the size of droplet. Suryo and Basaran (2006a; 2006b) conducted simulation with validated numerical model and concluded that the fluid temperature has effects on the droplet size. Sivasamy *et al.* (2014) performed numerical simulation with VOF method to investigate the droplet formation process in T-junction structure. Their model has been validated by the experimental results.

In this paper, the process of the dispersed phase being squeezed into droplets by continuous phase in a flow focusing structure is modeled with CLSVOF method. The influence of temperature on the size, shape and frequency of the droplet is investigated. In the numerical simulation, two types of liquid, water and oil, which are insoluble in each other, are assumed as dispersed phase and continuous phase respectively (Zhang *et al.*, 2017; Wu *et al.*, 2008). The influence of heating position on the formation of liquid droplets is investigated by keeping the velocity ratio of the two phases constant in the simulation. Although similar study has already been conducted by Nauyen *et al.* (2007), the present study has the following differences. First, the structure of the droplet generator adopted in this study is different. Second, instead of one heating position, multiply heating positions are considered and their influence on the droplets during the formation process are analyzed.

2. CONTROL MODELS

The numerical simulation on the microflow of the fluid is based on three governing equations, i.e., continuity equation, momentum conservation equation and energy conservation equation. The VOF model (Jiang, 2016) is widely used in the interphase insoluble multiphase flow problem, and the capillary number of the fluid is also an important parameter affecting the flow characteristics.

2.1 Continuity Equation

$$\frac{\partial \rho}{\partial t}+\nabla\cdot\left(\rho\vec{v}\right)=0 \tag{1}$$

where ρ is density, $\rho=\alpha_o\rho_o+\alpha_w\rho_w$, α_o,α_w are the phase fraction of oil phase, and water phase respectively, t is time, and $\vec{v}$ is velocity vector.

2.2 Momentum Conservation Equation

$$\frac{\partial}{\partial t}\left(\rho\vec{v}\right)+\nabla\cdot\left(\rho\vec{v}\vec{v}\right)=-\nabla p+\nabla\cdot\left(\bar{\bar{\tau}}\right)+\rho\vec{g}+\vec{F} \tag{2}$$

where p is static pressure, $\rho\vec{g}$ is fluid unit gravity vector, $\vec{F}$ is external force between phases (such as frictional effects, surface tension effects, and so on), and $\bar{\bar{\tau}}$ is stress tensor, derived from the following formula:

$$\bar{\bar{\tau}}=\mu\left[\left(\nabla\vec{v}+\nabla\vec{v}^{T}\right)-\frac{2}{3}\nabla\cdot\vec{v}I\right] \tag{3}$$

where μ is viscosity, $\mu=\alpha_o\mu_o+\alpha_w\mu_w$, μ_o,μ_w are oil and water viscosity respectively. I is unit tensor, the second term on the right-hand side in the bracket considers the effect of volume expansion.

2.3 Energy Conservation Equation

$$\frac{\partial(\rho E)}{\partial t}+\nabla\cdot(\vec{v}(\rho E+p))=\nabla\cdot[k_C(\nabla T)]+S_h \tag{4}$$

where E is energy, k_C is thermal conductivity,

$k_C = \alpha_o k_{Co} + \alpha_w k_{Cw}$; T is temperature; and S_h is energy source term (heat caused by the friction effect can be considered in this term).

2.4 VOF Model

The VOF model simulates the flow of two or more insoluble fluids by solving a single momentum equation and using the volume fraction of each fluid passing through the fluid domain. The phases in the VOF model are not intertwined with each other. For each additional phase added into the model, the volume fraction of the phase is introduced which in the controlled volume. In each controlled volume, the sum of the volume fraction of all phases equals 1. Therefore the volume fraction of phase q is α_q, then $\alpha_q = 0$ means that q phase is empty in the cell; the cell is filled with phase q when $\alpha_q = 1$, and $0 < \alpha_q < 1$indicates that the cell contains the interface between phase q and other fluid (Jiang *et al.*, 2018).

2.5 Level Set Method

The level set (LS) method is a simple and general method for calculating and analyzing the motion of interface in two dimensional or three-dimensional space proposed by Osher and Sethian (1988). The level set function is defined as a signed distance to the interface, and the level set function can be given as following:

$$\frac{\partial \varphi}{\partial t} + \nabla \cdot (\vec{v}\varphi) = 0 \tag{5}$$

The level set function φ is set to 0 in one phase and 1 in the other, varying from 0 to 1 near the interface, and is used to smooth the fluid parameters near the interface.

2.6 CLSVOF

The LS method can capture interface with high accuracy, however it is easy to lead to a poor volume conservation because of its numerical dissipation. On the other hand, the VOF method can preserve volume conservation, and its weakness is discontinuous across the interface. Therefore, they are used to combined each other, which is called CLSVOF (the coupled level set and volume of fluid method). In the CLSVOF method, volume conservation is achieved by solving the volume fraction equation. The interface is reconstructed by the VOF function, while the interface normal is calculated from the LS function. The LS function is re-distanced based on the reconstructed interface. Through the correction by the VOF function, the volume conservation can be accurately ensured.

2.7 Capillary Number

When droplets are formed in microchannels, the surface tension of droplets is the dominant force over gravity. The capillary number is a dimensionless value indicating the significance of surface tension. In the present study on droplet formation, the effect of temperature is considered. An analytical expression of capillary number as a function of temperature in 3D model was derived by Tan *et al.* (2008) based on the interphase shear rate in microtubules defined by Anna *et al.* (2006) and the expressions of temperature and viscosity derived by Nauyen *et al.* (2007) according to the relationship between temperature and interfacial tension. The expression of capillary number by Tan *et al.* (2008) is presented as follows:

$$Ca(T) = \frac{\mu_o a Q_c}{\gamma_o h}\left(\frac{1}{wz} - \frac{1}{b^2}\right)\exp(-0.02\Delta T) \tag{6}$$

where Ca is capillary number, μ_o is mineral oil viscosity ($0.0238 Pa\bullet s$ at 25°C), γ_o is interfacial tension between oil and water ($0.00365 N/m$ at 25°C), a is dispersion phase inlet radius, Q_c is flow of continuous phase, h is continuous phase inlet groove depth, b is continuous phase inlet radius, w is droplet shearing aperture, z is vertical distance from the top of the continuous phase aperture to the liquid drop shearing forming hole, and ΔT is temperature difference with respect to a reference T_0.

From Eq. (6), it can be concluded that the change of system temperature can affect capillary number, i.e., when the temperature increases, the capillary number decreases. From microscopic perspective, as the temperature increases, the molecular movement becomes increasingly active resulting in the decrease in the surface tension between oil and water. Such decrease in the interfacial tension causes the changes in frequency, shape and position of the droplet forming.

3. NUMERICAL MODELING

3.1 Geometry and Software

Figure 1 shows the geometry of the droplet generator considered in the numerical model of this paper. The area enclosed by dashed line is the heating area. In order to reduce the computation time and model size in the numerical simulation, only a small portion of the inlet region and upper water phase are modelled. P_W denotes the temperature at the heating position of dispersed phase, P_{OL} denotes the temperature of continuous phase at the left heating position and P_{OR} the temperature of continuous phase at the right heating position. The effect of heating on the water and oil inlet flows is realized by setting different values for dynamic viscosity and interfacial tension. The software for fluid analysis is Fluent 18.0. After the feasibility study on the grid number of the model, the simulation on the flow field is carried out with different working conditions. It takes about 14 hours to simulate the flow in the microtubule up to 40 *ms*. Photoshop CS6 is used to measure the size and position of each droplet under different working conditions after 40 *ms*. Each dimension of the droplets is analyzed and compared and the results are shown in a line chart plotted by Tecplot 2015.

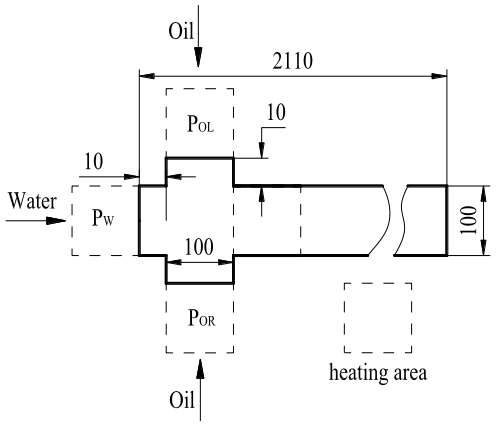

Fig. 1. Geometry of the droplet generator (μm).

3.2 Model Description

In this paper, the droplet formation due to the shear force generated by the flow focusing method is studied. The problem is modelled as a liquid-liquid two-phase flow with the continuous phase being oil and the dispersed phase being water. The viscosity and interfacial tension of the two phases at the selected temperature are presented in Table 1.

Table 1 Viscosity (mPa·s) and interfacial tension (mN/m) at different temperatures (°C)

Temperature	Water viscosity	Oil viscosity	Interfacial tension
10	1.3097	54.39	0.0041
20	1.0087	41.2	0.0038
30	0.8004	36.2	0.0036

The oil has a density of 998.2kg/m^3, a specific heat capacity of 1006.43J/(kg•K) and a thermal conductivity of 0.0242W/(m•K). The inflow velocity of oil in continuous phase is 0.0159m/s and that of water in dispersed phase is 0.00397m/s. The CLSVOF model is used for numerical simulation, and the energy equation is used for the consideration of different temperatures. The SIMPLE method is adopted for solving the pressure-velocity coupling. In space discretization, the least square method and PRESTO! are used for the gradient and the pressure calculation respectively. The momentum and energy equations are solved by the second order upwind scheme. Geo-Reconstruct is adopted to solve the volume fraction, and the first order upwind scheme is used for the level set function. The convergence factor of the energy equation is set to be 10e-6, and the convergence factor of the other equations is set to be 0.001. The relaxation factors are set by default, density is set to1, while pressure is 0.3, momentum is 0.7. The solution step size is set to be 10e-5s. The simulation takes 4000 steps. For each step, the maximum number of iterations allowable is 120.

The output values of Eq. (2) of the 4 steps among the first 20 steps are shown in Table 2

Table 2 Some output value of the Eq. (2)

Variables / Steps	Pressure (Pa)	U (m/s)	V (m/s)	LS Function
Initial	0	0	0	0
1	7.85e-06	2.90e-06	2.30e-04	2.33e-01
3	7.32e-04	5.19e-04	9.82e-04	1.10e-06
10	8.32e-04	3.05e-04	6.45e-04	5.46e-05
20	3.27e-04	2.41e-04	5.15e-04	5.40e-05

3.3 Mesh Sensitivity Verification

In the numerical simulation, meshing is needed to discretize the geometric model of the flow field. The larger the grids' number is, the more accurate the simulated flow field is (the smaller the mesh size is, the more uniform the droplet size is, the smoother the two-phase interface is (Jiang, *et al.*, 2018)). However, increasing in the grids' number will cause a sharp increase in computation cost, while the accuracy increases slowly. Therefore, it is important that the number of grids is within a reasonable range to achieve the balance between the computation efficiency and the cost. Figure 2(a) shows the mesh number and the computation time at different mesh sizes. The overall discretized fluid domain with a partial enlargement view at mesh size of 1.5μm is shown in Fig. 2(b). Figure 3 shows the diagrams of droplet phase at different mesh sizes after 2100 simulation steps.

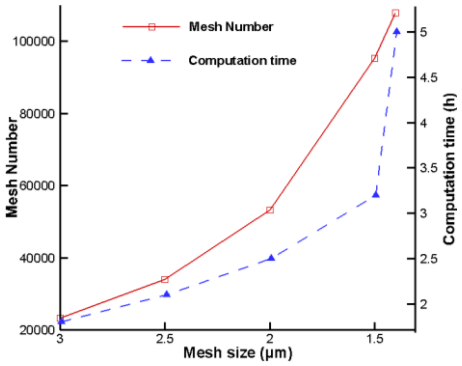

(a)

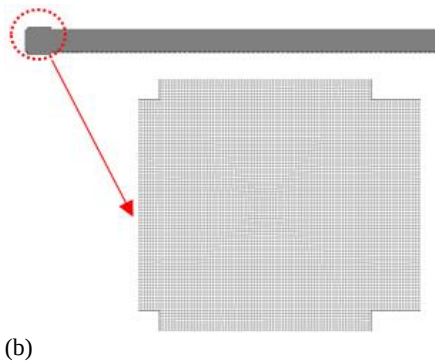

(b)

Fig. 2. (a) Mesh sensitivity analysis and (b) fluid domain discretized with mesh size of 1.5μm.

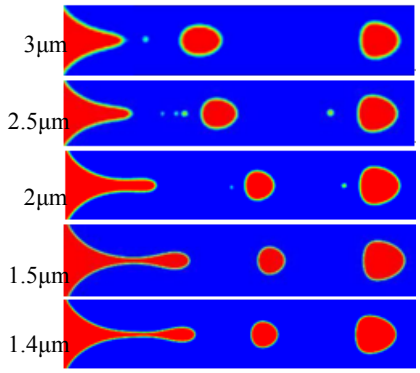

Fig. 3. Droplet phase contours at different mesh sizes after 2100 steps.

The solid line in Fig. 2(a) shows the relationship between the number of meshes and the mesh size in the simulated model. It can be seen that when the mesh size is reduced from 3μm to 1.4μm, the number of meshes increases nearly 5 times from 23364 to 107920. The dashed line shows the time the simulation takes to complete 2100 steps with different mesh sizes under the same boundary condition. It is seen that when the mesh size is reduced from 3μm to 1.4μm, the computation time increases nearly 180% from 1.8h to 5h. Therefore, it can be concluded from Fig. 2 that mesh size plays a key role in saving computation time. The accuracy of the numerical simulation is also affected by the size of the mesh. Figure 3 shows that the mesh size of the model has strong influence on the forming frequency and boundary regularity of the droplet when the model is numerically calculated under the same boundary condition. With the decrease of the mesh size, the droplet forming frequency increases, and the interface between formed water droplets and oil phase becomes more regular. When the mesh size is further reduced from 1.5μm to 1.4μm, the size and the forming frequency of droplets, as well as the regularity of the water-oil interface show little change, but the computation time increases nearly 1.6 times. Therefore, the mesh size of 1.5μm can meet the requirements of simulation for both accuracy and cost.

3.4 Simulation Cases

In their experimental analysis on the relationship between temperature and droplet formation, Tan *et al.* (2008) only considered the heating position where the droplet experienced maximum shear force in the microchannel. The initial temperature of the fluid in their experiment was 25°C, which was close to the room temperature. The fluid temperature was changed during the experiment and the law of droplet formation was analyzed. In this study, the influence of temperature on the droplet forming process was analyzed by considering heating at the inlets of both dispersed and continuous phases. In the numerical simulation, the initial global temperature is set to 10°C. The rang of heating temperature (that is, temperature difference) of both dispersed and continuous phases is from 10 to 30°C, at an interval of 10°C. For further analysis, the relevant symbols adopted in this paper are explained herein. Table 3 presents the simulation cases adopted in this paper. P_W, P_{OL} and P_{OR} are shown Fig. 1.

Table 3 Temperature of each case in the simulation

Case No.	Dispersed phase (P_W)	Continuous phase (P_{OL})	Continuous phase (P_{OR})
1	10	10	10
2	10	20	20
3	10	30	30
4	20	10	10
5	20	20	20
6	20	30	30
7	30	10	10
8	30	20	20
9	30	30	30
10	10	10	20
11	10	10	30
12	10	20	30
13	20	10	20
14	20	10	30
15	20	20	30
16	30	10	20
17	30	10	30
18	30	20	30

4. Results And Discussion

To validate the simulated results, a same model of Nauyen *et al.* (2008) is calculated and compared with the experimental results. Figure 4 represents the comparison of experimental data and the simulated data. The figure indicates a reasonable matching between the simulated results and the experimental data.

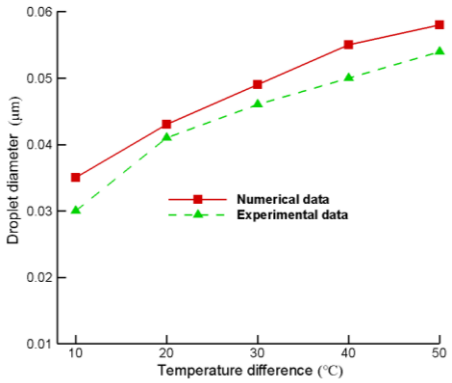

Fig. 4. Comparison of numerical and experimental results (Nauyen *et al.* (2008)) of droplet size at different temperature difference (Δ T), the initial temperature is 25°C, the inflow velocity of continuous phase is 0.0159m/s and that of dispersed phase is 0.00397m/s.

4.1 The Effect of Temperature on the Droplet Size and Formation Frequency

Figure 5 shows the size of droplets and pipe, in which, the droplets in the middle of microchannel are selected in order to eliminate the dimensional

errors caused by the large size change of the droplets due to the non-uniform surface tension during the droplet formation. Two droplets are used for the calculation of the droplet size. A dimensionless parameter E_T for the droplet size evaluation is defined as follows:

$$E_T = \frac{S_1 + S_2}{W} \tag{7}$$

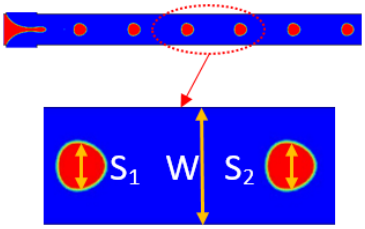

Fig. 5. Sketch of droplet and pipe size.

where T is dispersed phase temperature, S_1 and S_2 are the transverse dimension of the two droplets, and W is the width of the microchannel.

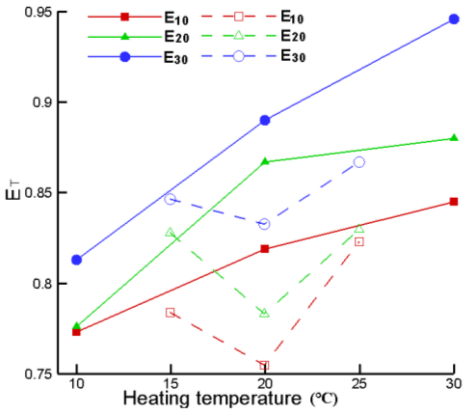

Fig. 6. Effects of temperature on the E_T, the heating temperature is 10°C-30°C, the inflow velocity of continuous phase is 0.0159m/s and that of dispersed phase is 0.00397m/s.

The influences of the temperature on the E_T is shown in Fig. 6, which the solid/dashed lines show the size of liquid droplet under different temperature of the dispersed phase with the temperatures of the left and right continuous phases being equal/unequal. E10, E20 and E30 indicate the size of droplet with the temperature of dispersed phase being 10°C, 20°C and 30°C. In Fig. 6, each solid line corresponds to one temperature of the dispersed phase. The horizontal axis is the temperature of continuous phase, and the vertical axis is the dimensionless parameter of droplet size E_T. It is can be seen from the solid lines in Fig. 6 that when the heating temperatures of the left and right continuous phase are equal, the higher the temperature of the dispersed phase, the larger the size of the liquid droplets generated by the device, the maximum increase of droplet size is 16%. Under constant temperature of dispersed phase, the size of liquid droplets generated by this device increases with the increase of the temperature of continuous phase.

The horizontal coordinate for the dashed line in Fig. 6 is the mean temperature at the inlet of the continuous phase (the average temperature being 15°C means the inlet temperature of the oil phase on the left/right side of the droplet generator is 10/20 °C; the average temperature being 20°C means the inlet temperature of both the left and the right oil phase is 20°C; the average temperature being 25 °C means the inlet temperature of the left/right oil phase is 20/30 °C). The dashed lines suggest that under the same average temperature, the droplet size increases with the increase of the temperature of the dispersed phase.

Through the comparison of solid and dashed lines, it can be seen that under the same dispersed phase temperature, the size of liquid droplets when the inlet temperatures of left and right oil phase are equal is larger than that when the left and right oil phases have different temperatures. The conclusion that the droplet size increases with the increase of the temperature of dispersed phase and continuous phase is consistent with the experimental results of Nauyen *et al.* (2007).

Figure 7 depicts a statistical diagram of the total number of droplets in each test group after 40 ms. When the number of droplets is counted, for the droplets not fully broken when the water phase flows through the shear point and enters the exit section, the following prescription is adopted. When the ratio of radial heights between the unbroken droplet and the former formed droplet is more than 1, it is counted as a complete droplet. When the radial ratio is between 0.5 and 1, 0.5 droplets is counted. For radial ratio less than 0.5, no droplet is counted.

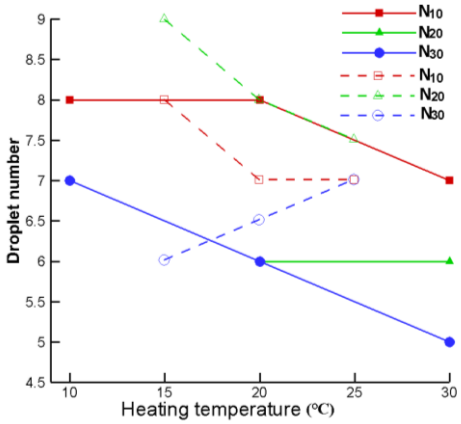

Fig. 7. Effects of temperature on the droplet numbers, the heating temperature is 10°C-30°C, the inflow velocity of continuous phase is 0.0159m/s and that of dispersed phase is 0.00397m/s.

The influences of the temperature on the droplet numbers is presented in Fig. 7, which the solid/dashed lines show the change in the number of droplets as the temperature of the dispersed phase increases, with the temperatures of the left and right continuous phases being equal/unequal, and the

droplet number at the temperature of dispersed phase being 10, 20 and 30°C is denoted as N_{10}, N_{20} and N_{30} respectively. It can be seen from the solid lines in Fig. 7 that when the heating temperatures of the left and right continuous phases are equal, the number of droplets increases with the decrease of the temperature of the dispersed phase, the biggest drop of droplets number is 29%. When the heating temperature of continuous phase varies, the number of droplets decreases with the increase of the temperature of the dispersed phase. From the dashed lines shown in Fig. 7, it can be seen that for each average heating temperature of continuous phase, the number of droplets at the temperature of dispersed phase being 20°C is higher than those at 10°C and 30°C. By comparing the solid and dashed lines, we can find that in general when the temperature of the dispersed phase is constant, the number of droplets decreases with the increase of the temperature of the continuous phase. However, for the dashed line with the temperature of the dispersed phase being 30°C, the number of droplets increases with the increase of the temperature of the continuous phase. The reason is that under this condition, the rule of droplet formation has changed. The number of droplets increases as the transition from the jetting regime to the dripping regime occurs with the increase of the continuous phase temperature. The mechanism of the droplets will be analyzed in section 4.4.

By comparison with Fig. 6 and Fig. 7, it is observed that for the simulation time considered, i.e. 40 ms, the size of liquid droplet is approximately inversely proportional to the number of droplets. Under the condition of constant velocity ratio of continuous phase to dispersed phase, with the increase of droplet size, the number of droplets decreases and the radial distance between the formed droplets increases. On the other hand, when the size of droplet decreases, the number of droplets increases and the radial distance between droplets decreases.

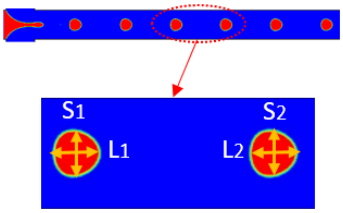

Fig. 8. Dimensions in the evaluation index of droplet shape.

4.2 The Effect of Temperature on the Droplet Shape

In Fig. 8, we select the droplet in the middle of the microtubule to calculate each dimension in the evaluation index of the droplet shape. Therefore, the error caused by the large change of the shape size due to the uneven surface tension during the formation of liquid droplet fracture is eliminated. Two droplets are chosen in the calculation of the dimension in order to reduce the error due to the inconsistent size of the droplets. In this section, the dimensionless roundness parameter C_T is adopted as an evaluation index of the droplet shape, as shown in Eq. (8):

$$C_T = \frac{S_1}{L_1} + \frac{S_2}{L_2} \tag{8}$$

where L_1 and L_2 are the radial dimension of the middle of the liquid droplet.

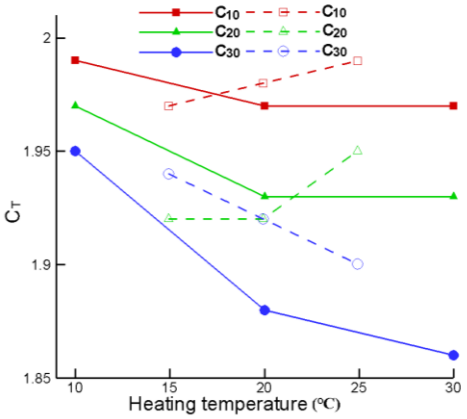

Fig. 9. Effects of temperature on C_T, the heating temperature is 10°C-30°C, the inflow velocity of continuous phase is 0.0159m/s and that of dispersed phase is 0.00397m/s.

The influences of the temperature on C_T is depicted in Fig. 9, which the solid/dashed lines demonstrate that when the heating temperatures of the left and right continuous phases are equal/unequal, the roundness parameter of the dispersed phase formed at different temperatures. C_{10}, C_{20} and C_{30} are evaluation index of droplet roundness at the temperature of 10°C, 20°C and 30 °C. If the droplet is a regular circle, the roundness parameter is equal to 2, otherwise the shape of droplet is not circular. Figure 9 show the roundness parameter of the formed droplets for each test group. It can be seen that no droplet with circular shape was formed under the conditions of the numerical simulation. Higher roundness parameter of the droplet is obtained under the condition of lower heating temperature at the inlets of both water and oil phases. From Fig. 9, it can be concluded that when the heating temperatures of the left and right continuous phases are equal, the higher the temperature of the dispersed phase, the smaller the roundness parameter of the formed droplet, the biggest drop of the roundness parameter is 5%, which indicates that the irregularity in the shape of droplet increases. When the temperature of the dispersed phase is constant and the heating temperatures of the left and right continuous phases are different, the roundness parameter of the droplet decreases with the increase of the average temperature of the continuous phase.

When the average heating temperatures of the left and right continuous phases are equal, the roundness parameter of the droplet formed at the dispersed phase being 10°C is higher than those formed at 20 and 30°C. As the average heating

temperature of the left and right continuous phases increases, the roundness parameters of the liquid droplets formed at dispersed phase being 10 and 20°C are higher than that formed at 30°C. It can also be found from Fig. 9 that when the average temperature of the left and right continuous phases is 20°C and the temperature of the dispersed phase being 10°C, the roundness parameter of the formed droplets is higher than those under other heating conditions with either the temperature or the average temperature of the continuous phases being 20°C.

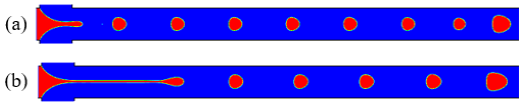

Fig. 10. Comparison of phase contours of liquid droplets. The heating temperature of the dispersed phase is 10°C. (a) The temperatures of both left and right continuous phases are 10°C. (b) The inlet temperature of the left and the right oil phase is 20 and 30 °C respectively.

When the temperature increases, the size of the droplet increases, and the transverse length of the upper part is much larger than that of the lower part, and the radial length is larger than that of the liquid droplet formed under the condition of lower temperature. In this case, the droplet shape is approximately inverted triangle, and the roundness parameter of droplet becomes smaller. The larger the droplet size, the smaller the roundness value, which is consistent with the trend as shown in Fig. 9.

4.3 The Effect of Temperature on Flow Regime

Derzsi *et al.* (2013) discovered and defined four dispersed phase flow regimes in their experiment. Among which the dripping regime is defined as the case that the liquid droplet breaks at or near the cross intersection and the tip of the droplet is retracted into the cross intersection after droplet breaking. The jetting regime is defined as that the dispersed phase passes through the intersection and goes deep into the exit of the microchannel. After the droplet breaks in the microchannel, the dispersed phase is still at the exit of the channel without bouncing back to the intersection.

In the liquid droplet generating device designed in this study, the velocity ratio of continuous phase to dispersed phase is constant. The liquid drop phase diagrams are obtained by changing the heating temperature at the inlet of the two phases. Two kinds of flow regime of the dispersed phase in this simulation have been observed as shown in Fig. 10: (a) dripping regime and (b) jetting regime.

In microflow, the capillary number determines the relative magnitude of viscosity and interfacial tension on the flow. Therefore, the capillary number is usually used to evaluate the dispersed phase flow regime in microflow. Figure 11 (a & b) show the capillary numbers of continuous and dispersed phases under different numerical simulation conditions. For the capillary numbers considered in Fig. 11, both dripping and jetting flow regimes are observed in this device. In Fig. 11(a), the horizontal coordinate is the capillary number of dispersed phases at heating temperature being 10°C, 20°C and 30°C, and the vertical coordinate is the capillary number of the left and right continuous phases at different heating temperatures.

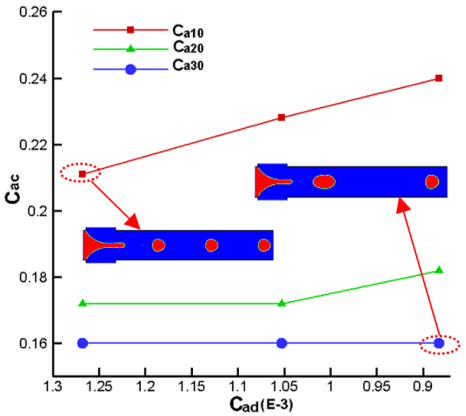

(a)

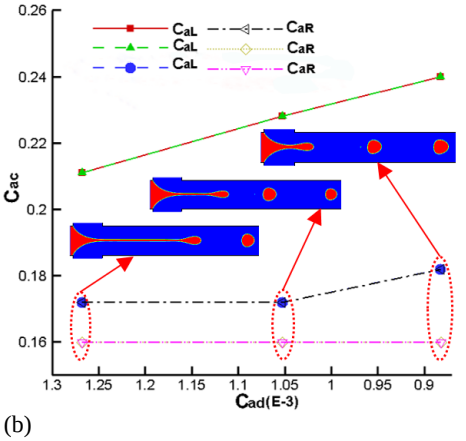

(b)

Fig. 11. Effects of C_{ad} on C_{ac}, the heating temperature is 10°C-30°C, the inflow velocity of continuous phase is 0.0159m/s and that of dispersed phase is 0.00397m/s.

In Fig. 11(a), the solid lines show the capillary numbers of the continuous phase with the change of the temperature of the dispersed phase, under the condition that the temperatures of the left and right continuous phases are equal. For all the nine sets of experiment under this condition, the flow regime of the dispersed phase is dripping, as shown in the droplet phase diagram in Fig. 11(a), and the shape and formation frequency of the droplet are different for different capillary numbers of dispersed and continuous phases. Comparing the droplet phase having capillary numbers of dispersed and continuous phases being 1.053E-3 and 0.211 respectively with the one having capillary numbers being 0.883E-3 and 0.16 for dispersed and continuous phases, it can be concluded that if the rest conditions are the same, the smaller the capillary numbers of dispersed and continuous phases, the larger the droplet size is, and the less the

droplets formed. In Fig. 11(b) Ca_L and Ca_R are the capillary number of the left and right continuous phases respectively at different heating temperatures. It can be seen from the graphs of the liquid droplets embedded in Fig. 11(b) that when the left and right continuous phases have different heating temperatures, there are two distinct jetting flow regimes of the dispersed phase for the nine sets of test conditions considered, while the remaining seven sets have dripping regime. The temperature of the continuous phase in the droplet phase diagram and elliptical dashed line demonstrates that when the temperatures of the left and right continuous phases are 20 and 30°C respectively, the larger the capillary number of the dispersed phase is, the more obvious the dispersed phase is in the jetting flow regime.

Under the dripping flow regime, the equilibrium between shear force and interfacial tension in the dispersed phase is considered, but the influence of inertial factor on the formation of droplets is neglected. As mentioned above, the capillary number of the continuous phase can describe the equilibrium between the shear force and the interfacial tension, when the capillary number of the continuous phase is small, the surface tension plays a leading role during flow focusing fracture to form droplets, and the breakpoint of droplet is cross intersection. Similarly, with the increase of capillary number, when the shear force gradually increases to overcome the surface tension during the droplet formation, the dispersed phase flow regime will change from dripping to jetting. Moreover, high viscosity of dispersed phase may deter the droplet formation, which promotes the flow regime transition from dripping to jetting.

The velocity field and temperature field of the calculated area are further analyzed. Figures 12-13 are velocity field of dripping flow and jetting flow.

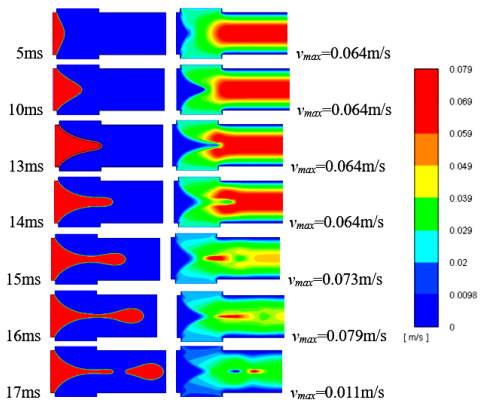

Fig. 12. Variation of velocity of dispersed phase and its surroundings during dripping flow.

Figure 12 shows t the dispersed phase contour and the velocity contour with dripping flow pattern. From the velocity contours from 5 to 14 ms, it can be seen that there is a high velocity region in the downstream section of the microchannel, i.e. the striped zone in red in the velocity contour, of which the velocity is exactly twice the inlet velocity of the continuous phase. Because initially the whole flow field region is filled with continuous phase, which enters the flow field uninterruptedly at certain velocity, the velocity in the middle of the flow field is the sum of the two velocities. As the viscosity of oil in the continuous phase is bigger, the shear force between the wall and the outflow section is bigger than that in the other areas of the flow field. The friction resistance exerted by the wall to the viscous fluid results lower velocity in the near wall than the velocity in other areas far away from the wall. The velocity gradient changes gradually in this state, which makes the velocity in the middle of the flow field the highest, and the velocity gradually decreases towards both sides. At 5 ms, the high-speed region of the continuous phase in the outflow section assumes a semicircular bulge, and the region gradually changes to a flat shape at 10 ms as the dispersed phase gradually flows into the channel. At 13 ms, the high-speed region of the outflow section is "sheared" into two halves as the dispersed phase gradually flows into the outflow section. The velocity at the tip of dispersed phase increases gradually and eventually becomes higher than that of the continuous phase. With the increase of the inlet time, the "high speed" region of the dispersed phase tip further enlarges till 14 ms. With the increase of the velocity, the droplets are stretched continuously, and the width of the droplet neck gradually decreases. When the width of the neck decreases to a certain value, the velocity of the dispersed phase droplets reaches the maximum in this micro-region, and the velocity of the upstream dispersed phase is far less than that of the micro-region, so the droplets break in this region. From the velocity contour at 17 ms, it can be seen that the tip velocity of the dispersed phase presents an obvious low velocity region immediately after fracture.

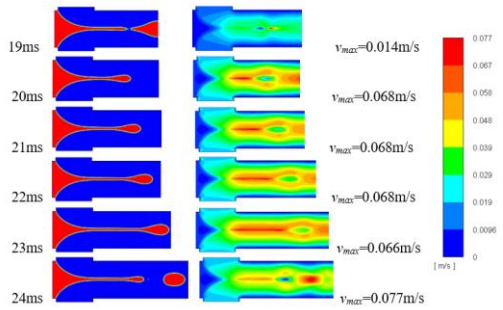

Fig. 13. Variation of velocity of dispersed phase and its surroundings during jetting flow.

Figure 13 shows the dispersed phase contour and the velocity contour with jetting flow pattern. As can be seen from the velocity contour at 19 ms, the velocity variation of the dispersed phase from the inlet to the breaking into droplets is generally consistent with the velocity variation of the droplet. At 20 ms, the velocity at the minimum neck width of the dispersed phase increases rapidly from about equal to that of the continuous phase to nearly two times, as shown in the red slender region in the figure. Under the action of viscous force, the

volume of the unbroken droplets in dispersed phase increases gradually with the new flow of the dispersed phase, and the radial length of the neck increases gradually. The radial distance at the outlet of the runner increases gradually, which is evident in the velocity contour from 20 to 23 ms. The velocity of the droplet increases gradually with the passing of time, and the velocity outside the droplet is larger than that inside the droplet. When the velocity outside the droplet increases gradually until equal to the velocity downstream of the droplet, the velocity at the tip of the droplet decreases sharply and the velocity at the minimum neck width decreases rapidly at the moment of breaking.

Figures 14-15 are temperature field of dripping flow and jetting flow.

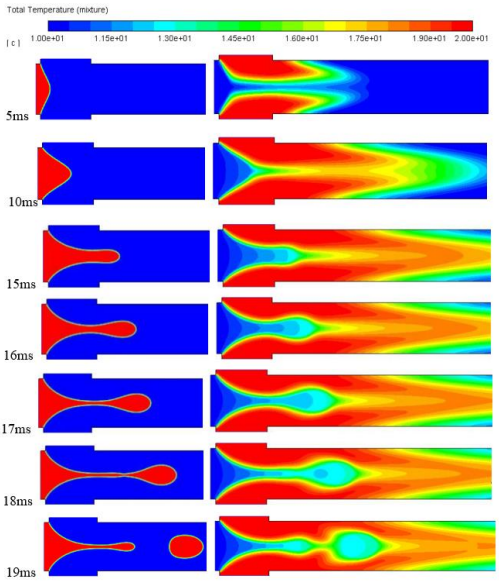

Fig. 14. Variation of temperature of dispersed phase and its surroundings during dripping flow.

Figure 14 shows the dispersed phase contour and the temperature contour with dripping flow pattern. When the temperature of continuous phase and dispersed phase is 10℃, the flow pattern of fracture of dispersed phase is trickle flow, but the change trend of temperature cannot be analyzed. Therefore, we select the case in which the temperature of continuous and disperse phases is 20 and 10 ℃, respectively. From the temperature contour at 5 ms, it can be seen that with the continuous phase being heated gradually and flowing into the intersection, the temperature in this region rises gradually, and the high temperature region flows to the outflow section and intersects gradually with the flow of dispersed phase. It can be seen from the temperature contours from 15 to 17 ms that as the volume of the droplet in the unbroken dispersion and the radial distance of the neck gradually increase, the temperature inside the droplet gradually increases. From the temperature contour at 18 ms, it can be seen that the temperature inside the droplet gradually increases to the same as the surrounding temperature after the droplet breaks.

Figure 15 shows the dispersed phase contour and the temperature contour with jetting flow pattern. The red, green and blue region in the temperature contour of the continuous phase has temperature being 30, 20, and 10℃, respectively. As can be seen from the temperature contour at 19 ms, the temperature change of the dispersed phase from the inlet to the breaking into droplets is generally consistent with the temperature change of the droplet.

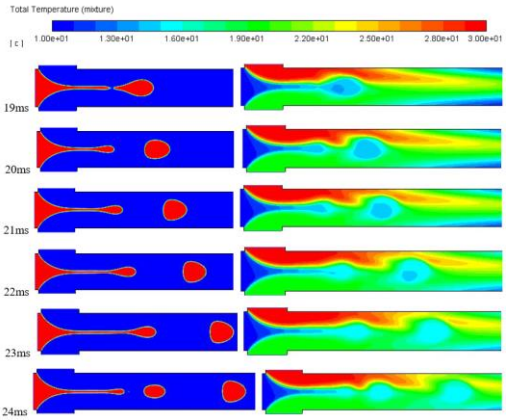

Fig. 15. Variation of temperature of dispersed phase and its surroundings during jetting flow.

From 19 to 22 ms, the shape of the formed droplets is smooth in the low temperature region near the low temperature side, and the range of the low temperature region decreases gradually as the temperature rises, and the shape of the broken droplets tends to be uniform.

4.4 The Effect of Temperature on Droplet Formation

Figure 16 shows the comparison of the formation of droplets since the fracture in the dripping and jetting flow regimes. From Fig. 16(a), it can be seen that in the dripping flow regime, breakup point is located in the intersection part but very close to the intersection. After the droplet breaks up from the fracture point, its upper part shrinks to a sharp point due to the tension before fracture. The lower part of the droplet is oval due to surface tension. With the tension in the upper part fading away, the sharp point of droplet becomes blunt, which makes the surface tension of the droplet distribute more evenly. Also, the droplet is subjected to the inertia force in Y direction. Therefore, the droplet has slightly larger deformation in its upper part than in its lower part, which makes the droplet peach-like in its final shape.

From the dripping flow regime depicted in Fig. 16(a), we can see that there are three stages in droplet re-formation, i.e., fluid aggregation stage, necking stage, and fracture stage. The dispersed phase sheared by continuous phase gradually flows into the intersection. The tip point of the upper dispersed phase at the intersection gradually expands outward into a column because of the inflow of fluid, and the tip point disappears. At this

time, the droplet formation enters the second stage. In the necking stage, with the continuous inflow of fluid, the front end of the column of dispersed phase gradually expands outward into an ellipse under the action of surface tension. With the expansion of the lower ellipse of the droplet, the neck of the droplet becomes narrower and narrower. When the neck shrinks to a point, the droplet formation enters the fracture stage, in which the fracture occurs and the new droplet is formed.

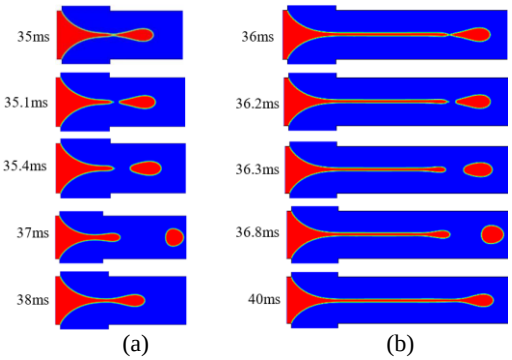

Fig. 16. Comparison of droplet formation in dripping and jetting flow regimes. The heating temperature of the dispersed phase is 10°C, (a) indicates that the temperatures of the left and right continuous phase are 10°C, and (b) presents that inlet temperature of left and right oil phases is 20 and 30°C, respectively.

Figure 16(b) indicates the formation and variation of droplets under jetting flow regime. It can be seen from the phase diagram that the droplet shape in the microchannel after fracture is almost the same as that in the dripping flow regime with the increase of time. However, the breakpoints of the droplets in the two flow regimes are quite different, in which the fracture point of jetting flow regime extends to the exit section. When the temperature of the dispersed phase is 10°C, and the inlet temperature of the two continuous phases is 20°C and 30°C, respectively, the radial distance between the fracture point and the exit section is more than 2 times the diameter of the pipe, which is much larger than the radial distance of the fracture point under the dripping flow regime. The process of droplet formation out of the fine filamentous dispersed phase in the outflow section is also divided into three stages: fluid aggregation stage, necking stage, and fracture stage. The biggest difference between the jetting flow regime and the dripping flow regime at this stage is that after the droplet breaks at the fracture point, the filamentous dispersed phase bounces back in a short distance towards the entrance of the dispersed phase, which is caused by the viscoelasticity of the dispersed phase.

4.5 The Effect of Temperature on Droplet Breakup Location

The location and dimension of the droplet breakup point is shown in Fig. 17, and the comparison results are depicted in Fig. 18. From Fig. 17, "L" is the measurement of the flow direction of the position. In Fig. 18 the horizontal axis is the heating temperature of continuous phase, and the vertical axis is the radial dimension of the breakup position of the droplet. The solid and the dashed lines correspond to the condition that the temperatures of the left and right continuous phase are equal and the temperature of the dispersed phase is constant. The dash dot and the dotted lines correspond to the condition that the heating temperatures of the left and right continuous phases are not equal and the temperature of the dispersed phase is constant. When the temperature of dispersed phase is constant, the radial dimensions of different droplet fracture points are different. It can be seen from Fig. 18 that the radial dimension of the fracture point of the first droplet is larger than that of the fifth regardless of whether the heating temperatures of the continuous phases are equal or not. As the heating temperature of the dispersed phase is constant and the inlet temperatures of the left and right continuous phases gradually increase, the radial dimension of the fracture point gradually reduces, meaning the fracture point of the droplet is more and more close to the cross intersection. However, it can be found from the values of radial dimension in Fig. 18 that when the dispersed phase is a jetting flow regime (as presented by the dotted ellipse in Fig. 18), the radial dimension of the fracture point gradually decreases while that in the jetting flow regime gradually increases and restabilizes.

Fig. 17. Location and dimension of the droplet breakup point. The heating temperature of the dispersed phase is 10°C, the inlet temperature of the left and right oil phases is 20 and 30 °C, respectively.

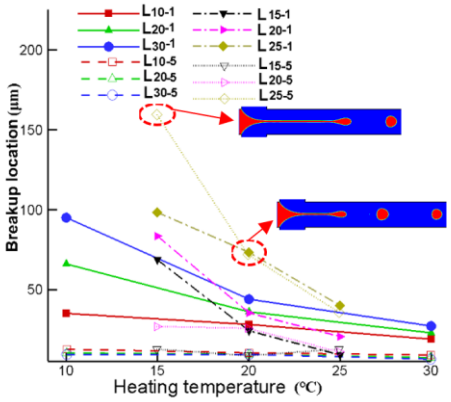

Fig. 18. Comparison of the radial dimension of the first and fifth droplets' fracture points in each test group, $L_{T\text{-}i}$ is shown at different temperatures for the droplet breakup location, *T* is the dispersed phase temperature and *i* is the liquid drop.

As a whole, the radial dimension of the droplet fracture point decreases to a stable value with the increase of temperature and is generally larger than that of the fifth droplet. Because the initial oil phase temperature is 10℃ in this numerical simulation, the capillary number of continuous phase is relatively low, so the fracture point of dispersed phase assumes a transient jetting flow regime at the beginning. As the capillary number increases with the increase of temperature, the droplet dispersion phase gradually transforms into dripping flow regime, and the radial dimension of fracture point of the first droplet is generally larger than that of the fifth droplet.

5. CONCLUSIONS

In this paper, by changing the heating temperature at the inlet of dispersed phase and continuous phases in the flow focusing structure, the effects of temperature on the size, forming frequency, shape of droplets, and flow regime, droplet formation are analyzed.

(1) The CLSVOF model of microflow is built, and the analytical parameter E_T, C_T are defined, they are effective tools for quantitative analyzing the influence of temperature on droplet on droplet forming.

(2) With the increase of temperature, the size of the droplet increases and the frequency of the droplet decreases.

(3) When the temperature of the dispersed phase is constant and the temperatures of the left and right continuous phases are equal, the irregularity of the formed droplets increases with the increase of the temperature. When the temperature of the dispersed phase is constant and the temperatures of the left and right continuous phases are different. The irregularity of formed droplets reduces with the increase of the temperature;

(4) The dispersed phase represents dripping flow regime when the temperatures of the left and right continuous phases are equal. As the temperatures of the continuous phases are not equal, the disperse phase represents jetting flow regime if the capillary number of the continuous phase is low, and represents dripping flow regime if the capillary number is slightly high. The velocity and temperature field under different flow regime are discussed.

(5) Under the dripping flow regime, the radial dimension of the droplet fracture point decreases to a stable value with the increase of the heating temperature of the continuous the dispersed phases, while under the jetting flow regime, the radial dimension of the droplet fracture point gradually increases to a stable value with the increase of the heating temperatures of the continuous and the dispersed phases.

(6) More experimental verification is needed in the future, and the friction effects and other factors should be considered.

ACKNOWLEDGEMENTS

The modelling support from www.simulationdirect.com is appreciated. gratefully acknowledge research support from the Natural Science Foundation of Guangdong Province (2016A030313653) and the Science and Technology Plan of Guangzhou City (201607010291).

REFERENCES

Abou-Hassan, A., O. Sandre and V. Cabuil (2010). Microfluidics in inorganic chemistry. *Angewandte Chemie International Edition* 49(36), 6268-6286.

Anna, S. L. and H. C. Mayer (2006). Microscale tipstreaming in a microfluidic flow focusing device. *Physics of Fluids* 18(12), 121512.

Basova, E. Y. and F. Foret (2015). Droplet microfluidics in (bio) chemical analysis. *Analyst* 140(1), 22-38.

Bedram, A. and A. Moosavi (2013). Breakup of droplets in micro and nanofluidic T-junctions. *Journal of Applied Fluid Mechanics* 6(1), 81-86.

Bruijns, B., A. V. Asten, R. Tiggelaar and H. Gardeniers (2016). Microfluidic Devices for Forensic DNA Analysis: A Review. *Biosensors* 6(3), 41-75.

Christopher, G. F. and S. L. Anna (2007). Microfluidic methods for generating continuous droplet streams. *Journal of Physics D Applied Physics* 40(19), 319-336.

Chwalek, J. M., D. P. Trauernicht, C. N. Delametter, R. Sharma and D. L. Jeanmair (2002). A new method for deflecting liquid microjets. *Physics of Fluids* 14(6), 37-40.

Derzsi, L., M. Kasprzyk, J. P. Plog and P. Garstecki (2013). Flow focusing with viscoelastic liquids. *Physics of Fluids* 25(9), 368-141.

Eslamian, M. and N. Ashgriz (2011). *Drop-on-Demand Drop Generators*. In N. Ashgriz (ed.), Handbook of Atomization and Sprays, *Springer*, 581-601.

Evanko, D. (2008). Living droplets. *Nature Methods* 5(7), 580-581.

Fabian, M., P. Burda, M. Šviková and R. Huňady (2016). The Influence of magnetic field on the separation of droplets from ferrofluid jet. *Journal of Magnetism & Magnetic Materials* 431, 196-205.

Hung, L. Y., C. H. Wang, C. Y. Fu, P. Gopinathan and G. B. Lee (2016). Microfluidics in the selection of affinity reagents for the detection

of cancer: paving a way towards future diagnostics. *Lab on a Chip* 16(15), 2759-2774.

Jahn, A., J. E. Reiner, W. N. Vreeland, D. L. DeVoe, L. E. Locascio and M. Gaitan (2008). Preparation of nanoparticles by continuous-flow microfluidics. *Journal of Nanoparticle Research* 10(6), 925-934.

Jiang, F., Y. C. Xu and P. Huang (2018). *Fluent advanced application and case study*. Tsinghua University Press: China.

Jiang, F., Y. Long, Y. J. Wang, Z. Z. Liu and C. G. Chen (2016). Numerical simulation of non-Newtonian core annular flow through rectangle return bends. *Journal of Applied Fluid Mechanic* 9(1), 431-441.

Li, S., J. Xu, Y. Wang and G. Luo (2008). Controllable preparation of nanoparticles by drops and plugs flow in a microchannel device. *Langmuir* 24(8), 4194-4199.

Mashaghi S., A. Abbaspourrad, D. A. Weitz and A. M. V. Oijen(2016). Droplet microfluidics: A tool for biology, chemistry and nanotechnology. *Trends in Analytical Chemistry* 82, 118-125.

Neethirajan, S., I. Kobayashi, M. Nakajima, D. Wu, S. Nandagopal and F. Lin (2011). Microfluidics for food, agriculture and biosystems industries. *Lab on a Chip* 11(9), 1574-1586.

Osher, S. and J. A. Sethian (1988). Fronts propagating with curvature-dependent speed: Algorithms based on Hamilton-Jacobi formulations. *Journal of Computational Physics* 79(1), 12-49.

Price, A. K. and B. M. Paegel (2015). Discovery in Droplets. *Analytical Chemistry* 88(1), 339.

Qiu, D., L. Silva, A. L. Tonkovich and R. Arora (2010). Micro-droplet formation in non-Newtonian fluid in a microchannel. *Microfluidics & Nanofluidics* 8(4), 531-548.

Schneider, T., J. Kreutz and D. T. Chiu (2013). The potential impact of droplet microfluidics in biology. *Analytical Chemistry* 85(7), 3476-3482.

Sivasamy, J., T. N. Wong, N. T. Nguyen and T. H. Kao (2014). An investigation on the mechanism of droplet formation in a microfluidic T-junction. *Microfluidics & Nanofluidics* 14(1), 1-10.

Song, Y., J. Hormes and C. S. S. R. Kumar (2010).Microfluidic Synthesis of Nanomaterials. *Small* 4(6), 698-711.

Suryo, R. and O. A. Basaran (2006a). Dripping of a Liquid from a Tube in the Absence of Gravity. *Physical Review Letters* 96(3), 034504.

Suryo, R. and O. A. Basaran (2006b). Tip streaming from a liquid drop forming from a tube in a co-flowing outer fluid. *Physics of Fluids* 18(8), 289-79.

Tan, S. H., M. S. M. Sohel, N. T. Nguyen, T. N. Wong and L. Yobas (2008). Thermally controlled droplet formation in flow focusing geometry: formation regimes and effect of nanoparticle suspension. *Journal of Physics D Applied Physics* 41(16), 2444-2454.

Teo, A. J. T., K. H. H. Li, N. T. Nguyen, W. Guo, N. Heere, H. D. Xi, C. W. Tsao, W. Li and S. H. Tan (2018). Negative pressure induced droplet generation in a microfluidic flow-focusing device. *Analytical Chemistry* 89(8), 4387-4391.

Theberge, A. B., F. Courtois, Y. Schaerli, M. Fischlechner, C. Abell, F. Hollfelder and W. T. S. Huck (2010). ChemInform Abstract: Microdroplets in Microfluidics: An Evolving Platform for Discoveries in Chemistry and Biology. *Angewandte Chemie International Edition* 41(45), 5846-5868.

Vyawahare, S., A. D. Griffiths and C. A. Merten (2010). Miniaturization and Parallelization of Biological and Chemical Assays in Microfluidic Devices. *Chemistry & Biology* 17(10), 1052-1065.

Wang, X. D., C. Y. Zhu, T. T. Fu, T. Qiu and Y. G. Ma (2017). Critical condition for bubble breakup in a microfluidic flow-focusing junction. *Chemical Engineering Science* 164(2), 178-187.

Wu, L., M. Tsutahara, L. S. Kim and M. Y. Ha (2008). Numerical simulations of droplet formation in a cross‐junction microchannel by the lattice Boltzmann method. International *Journal for Numerical Methods in Fluids* 57(6), 793-810.

Xu, J. H., S. W. Li, J. Tan and G. S. Luo (2008). Correlations of droplet formation in T-junction microfluidic devices: from squeezing to dripping. *Microfluidics & Nanofluidics* 5(6), 714-717.

Zec, H., D. J. Shi and T. H. Wang (2014). Novel droplet platforms for the detection of disease biomarkers. *Expert Review of Molecular Diagnostics* 14(7), 787-801.

Zhang, C., T. T. Fu, C. Y. Zhu, S. K. Jiang, Y. G. Ma and H. Z. Li (2017). Dynamics of bubble formation in highly viscous liquid in a flow-focusing device. *Chemical Engineering Science* 172 (6), 278-285.

Zhu P. A. and L. Q. Wang (2017). Passive and active droplet generation with microfluidics: a review. *Lab on a Chip* 17(2), 34-75.